Reverse droop control-based smooth transfer strategy for interface converters in hybrid AC/DC distribution networks

Cao, Wenyuan; Han, Minxiao; Xie, Wenqiang; Meng, Xiangkun ; Khan, Zmarrak Wali ; Guerrero, Josep M.; Tinajero, Gibran David Agundis

Published in:
CSEE Journal of Power and Energy Systems

DOI (link to publication from Publisher):
10.17775/CSEEJPES.2020.02070

Publication date:
2023

Document Version
Publisher's PDF, also known as Version of record

Reverse Droop Control-Based Smooth Transfer Strategy for Interface Converters in Hybrid AC/DC Distribution Networks

Wenyuan Cao, *Student Member, IEEE*, Minxiao Han, *Member, CSEE, Senior Member, IEEE*, Xiangkun Meng, Wenqiang Xie, Zmarrak Wali Khan, *Student Member, IEEE*, Josep M. Guerrero, *Fellow, IEEE*, and Gibran Agundis-Tinajero, *Member, IEEE*

***Abstract*—Hybrid AC/DC distribution networks are promising candidates for future applications due to their rapid advancement in power electronics technology. They use interface converters (IFCs) to link DC and AC distribution networks. However, the networks possess drawbacks with AC voltage and frequency offsets when transferring from grid-tied to islanding modes. To address these problems, this paper proposes a simple but effective strategy based on the reverse droop method. Initially, the power balance equation of the distribution system is derived, which reveals that the cause of voltage and frequency offsets is the mismatch between the IFC output power and the rated load power. Then, the reverse droop control is introduced into the IFC controller. By using a voltage-active power / frequency-reactive power (*U-P / f-Q*) reverse droop loop, the IFC output power enables adaptive tracking of the rated load power. Therefore, the AC voltage offset and frequency offset are suppressed during the transfer process of operational modes. In addition, the universal parameter design method is discussed based on the stability limitations of the control system and the voltage quality requirements of AC critical loads. Finally, simulation and experimental results clearly validate the proposed control strategy and parameter design method.**

***Index Terms*—Hybrid AC/DC distribution network, interface converters, reverse droop control, adaptive adjustment, parameter design method.**

I. Introduction

THE DC distribution network has become a promising alternative to the AC network due to the rapid development of DC power supplies and loads. It has many advantages, such as lower line losses, enhanced controllability and easy access to clean energy [1], [2]. However, AC networks still have many applications which are completely irreplaceable. Therefore, the development of hybrid AC/DC systems is the most optimal solution for future distribution networks. The flexible connection and coordinated operation of AC and DC distribution networks have great importance in the development of the hybrid distribution network [3], [4]. Nethertheless, it is important to carry out flexible power transmission between individual AC and DC networks under the grid-tied mode. The system also requires that the DC distribution network supply uninterrupted power to the critical AC loads under the islanding mode [5].

In order to achieve smooth transfer between the grid-tied mode and islanding mode, two types of control strategies are proposed: hybrid voltage-current source control [6]-[11] and voltage source control [12]-[14].

In a hybrid voltage-current source control, the IFC is controlled as a current source under the grid-tied mode to maintain power exchange between the AC and DC distribution networks. On the other hand, when islanding is detected, the IFC is switched to be controlled as a voltage source. Thus, the voltage and frequency of the critical AC loads are provided by the IFC under islanding mode. Taking advantage of the use of two different control strategies, the distribution network under the hybrid voltage-current source control can operate at high efficiency in both modes. However, the islanding detection always takes tens of milliseconds to several seconds [15]-[17], during which the IFC remains in the current source mode, although the AC main network is disconnected. In this case, the mismatch between the IFC output power and the rated load power will cause fluctuations in the magnitude and frequency of the critical load voltage. Even more serious scenarios can be found, for example, if the IFC is set to inject a constant active power from the AC network into the DC network under the grid-tied mode, the AC voltage will be unstable during the islanding detection delay, since there is no power support from the AC side [18]. In conclusion, the conventional hybrid voltage-current source control-based strategies face difficulties to achieve continuous control of the AC load voltage. In this way, some recent research studies [6]-[8] have proposed several advanced control strategies, such as model predictive control (MPC) [6], [7] and observer-based control (OBC) [8]. Although they achieve seamless transfer between operating modes, these strategies sacrifice the simplicity of the control system and are susceptible to noise. Additionally, some researchers proposed strategies based on indirect current

This work was supported by the National Key R&D Program of China (2018YFB0904700).

W. Cao, M. Han, X. Meng, W. Xie and Z. Khan are with the School of Electric and Electronic Engineering, North China Electric Power University, Beijing 102206, China(e-mail:18173528776@163.com; hanminxiao@263.net; mengxk321@163.com;bjxiewenqiang@163.com;zmarrakwali@outlook.com).

J. M. Guerrero and Gibran Agundis-Tinajero are with the Department of Energy Technology, Aalborg University, Aalborg 9220, Denmark (e-mail: joz@et.aau.dk; gdat@et.aau.dk).

DOI: 10.17775/CSEEJPES.2020.02070

control to solve this issue [9]-[11]. Different from the conventional direct current control-based strategies which use the outer voltage loop and inner current loop, the indirect current control-based strategies adopt the outer current loop and inner voltage loop under the grid-tied mode. With these strategies, the outer current loop control is removed while the inner voltage loop control remains operational under islanding mode. In this way, the load voltage is always controlled as the inner voltage loop is maintained throughout the whole process. Therefore, the voltage quality can be significantly improved during the islanding detection delay. Nevertheless, there are still several drawbacks to these indirect current control-based strategies. The dynamic response of the current is slow and the quality of the current waveform is relatively poor due to the absence of the current loop control.

The voltage source control always controls the IFC as a voltage source. Under this control mode, a *P-f* / *Q-U* droop loop or a *Q-f* / *P-U* droop loop is usually added to the traditional dual control loop, which realizes the control of both frequency and voltage [12]-[14]. In such a case, the switching of control strategies is eliminated. However, the offsets of voltage magnitude and frequency increase due to the voltage droop and frequency droop loop [12]. In addition, this method faces difficulty to achieve free transmission of power under the grid-tied mode, which sacrifices the flexibility and efficiency of the hybrid AC/DC distribution network. Although the droop loop can be modified to achieve constant power control of the IFC under the grid-tied mode in [13], this is at the cost of introducing the switching of the control strategies. Similarly, a unified control structure was proposed to achieve multi-mode operation and smooth transfer in [14], however, the upper layer control still requires different reference values under different modes of operation.

In summary, the hybrid voltage-current source control can achieve efficient operation of the hybrid AC/DC distribution network, but the voltage quality during the islanding detection delay is poor. On the other hand, the voltage source control has a good voltage quality during the islanding detection delay, but it faces difficulties to achieve an efficient operation. Inspired by the reverse droop control proposed to realize proper power sharing in [19], [20], this paper developes a new form of voltage-active power / frequency-reactive power (*U-P* / *f-Q*) reverse droop control to achieve a smooth transfer between the grid-tied mode and islanding mode for IFCs. In fact, the proposed *U-P* / *f-Q* reverse droop control is the reverse of *Q-f* / *P-U* droop [21], [22]. The *Q-f* / *P-U* droop control generates voltage and frequency reference signals, and it is used to control the grid-forming IFCs. However, the proposed *U-P* / *f-Q* reverse droop control generates active power and reactive power reference signals, so it is used to control the grid-following IFCs. Therefore, the *Q-f* / *P-U* droop control is used in voltage source control, whereas the proposed *U-P* / *f-Q* reverse droop control is adopted to replace the constant power control in a traditional hybrid voltage-current source control. With this control, the IFC output power will adaptively adjust to the rated load power by following the droop curve when islanding occurs. Hence, the magnitude and frequency of AC voltage can be maintained within an allowable range. Even if the islanding detection delay is relatively long, the uninterrupted and qualified power supply for the critical loads can be achieved.

The main contributions of this paper can be summarized as follows:

1) Proposing a new form of reverse droop control to achieve a smooth transfer between the grid-tied mode and islanding mode. The operating principle of the proposed control is described in detail.

2) Presenting a unified parameter design method for the IFC controller, during which the small-signal stability of the system is analyzed.

The rest of this paper is organized as follows: In Section II, the schematic diagram of the AC/DC distribution system is introduced. Section III proposes the reverse droop control by deducing the relationship between the load voltage magnitude, frequency and load power. Also, the operating principle is discussed in detail and the control diagram is demonstrated. In Section IV, first, the calculation formulas of the current loop and the voltage loop compensator parameters are presented. Then, according to the stability analysis and power quality requirements, the design method of the droop coefficients is given. Section V verifies the proposed control strategy and parameter design method by simulation and experimental results. Finally, the conclusions are depicted in Section VI.

II. Schematic of the AC/DC Distribution System

The basic structure of the AC/DC distribution system connected by an IFC is shown in Fig. 1. Where L_f is the filter inductor, C_f is the filter capacitor, R_f denotes the resistance of the filter inductor, Z_L shows the impedance of the critical loads, S_c and S_g depict the switches that are controlled by the IFC and main grid respectively. The IFC can be a two-level voltage-sourced converter, a three-level voltage-sourced converter, or a modular-multilevel converter, depending on its application scenario and the voltage level.

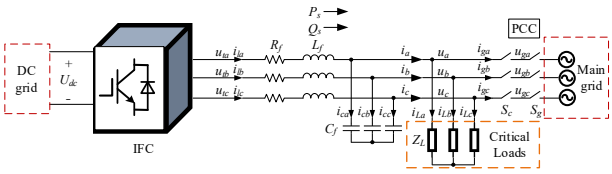

Figure 1. Schematic of the AC/DC distribution system.

III. The Proposed Strategy Based On Reverse Droop Control

A. Operating Principle of the Current Source Control under Islanding Mode

For a hybrid voltage-current source control, the IFC is controlled as a current source under the grid-tied mode. The unified circuit is shown in Fig. 2 [15]. Here, P_g and Q_g are the power flowing into the main grid, while, P_L and Q_L show the power consumed by the critical loads, P_s and Q_s are IFC output power.

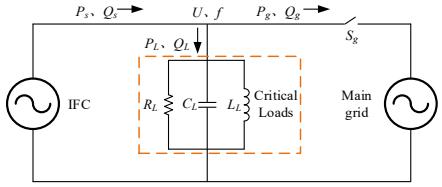

Fig. 2. The unified circuit with the power flow when the IFC is controlled as a current source.

According to Fig.2, the power dissipated in the critical loads under the grid-tied mode can be represented as:

$$\begin{cases} P_{L0} = \dfrac{U_0^2}{R_L} \\ Q_{L0} = U_0^2\left(\dfrac{1}{2\pi f_0 L_L} - 2\pi f_0 C_L\right) \end{cases} . \tag{1}$$

Where U_0 and f_0 are the rated voltage and rated frequency of the load, P_{L0} and Q_{L0} represent the rated power of the load. Due to the dispersed critical loads, P_{L0}+jQ_{L0} is difficult to measure but can be simply calculated by P_{L0}+jQ_{L0}=P_{s0}+jQ_{s0}-(P_{g0}+jQ_{g0}). Where P_{s0}+jQ_{s0} and P_{g0}+jQ_{g0} show the output power of the IFC and the power injected into the main grid under the grid-tied mode, respectively.

At the occurrence of islanding (i.e., S_g is off), the IFC control strategy does not instantly switch due to an islanding detection delay. In such a case, P_g+jQ_g=0 and the total power generated by the IFC is all consumed by the loads, i.e., P_s+jQ_s=P_L+jQ_L. Then the relationship of the IFC output power with load voltage and frequency is given as:

$$\begin{cases} P_s = P_L = \dfrac{U^2}{R_L} \\ Q_s = Q_L = U^2\left(\dfrac{1}{2\pi f L_L} - 2\pi f C_L\right) \end{cases} . \tag{2}$$

Where U and f are the actual load voltage magnitude and frequency, respectively. Equation (2) indicates that U and f suffer from the mismatch between the IFC output power and rated load power. In this case, U and f will increase if P_s> P_{L0} and Q_s<Q_{L0}. Otherwise, U and f will be suppressed. It can also be seen that U is determined by P_s, whereas f primarily relies on Q_s.

B. *Proposed Reverse Droop Control*

According to (2), U and f can be determined by adjusting the P_s and Q_s independently. Therefore, a *U-P* / *f-Q* reverse droop control for the current source control is proposed here. The governing equation for reverse droop control is formulated as:

$$\begin{cases} P_s^* = P_{s0} - m(U - U_0) \\ Q_s^* = Q_{s0} + n(f - f_0) \end{cases} \tag{3}$$

Where m and n denote the droop coefficients of voltage and frequency, P_s^* and Q_s^* are the reference power of the IFC, P_{s0} and Q_{s0} are the desired output power of the IFC under the grid-tied mode.

Under the grid-tied mode, U and f are clamped to U_0 and f_0 by the main grid, i.e., the output power of the IFC is P_{s0}+jQ_{s0} according to (3). After the occurrence of islanding, a schematic diagram of the adaptive adjustment process of the active power based on (2) and (3) is shown in Fig. 3. Fig. 3(a) demonstrates the adjustment process when P_{s0}>P_{L0}. In such a case, the load operates at point A and absorbs P_{L0}, the IFC initially generates P_{s0}. When islanding is activated, P_L instantaneously increases from P_{L0} to P_{s0}, causing the loads operating point to move from A to B and U rises, as depicted in ① and ②. If the conventional constant power control is applied, the load will always operate at point B, which means U deteriorates during the whole islanding detection delay. Whereas if the proposed droop control is employed, the increase of U will cause P_s^* to decrease, thereby P_s and P_L are minimized to adaptively reduce the voltage offset, the load will operate from point B to point C, as portrayed in ③ and ④. Eventually, the load will converge to operate at point O, where the load voltage is U_O and the IFC output active power is P_O. The active power adaptive adjustment process when P_{s0}<P_{L0} is exhibited in Fig. 3(b), where the load will also adapt to operate at point O. The motor load [23]-[25] can also be included in the unified circuit shown in Fig. 2 but with a variable R_L. Since the variable R_L only affects the slope of the curve that corresponds to equation (2), the system will converge to the operating point O no matter how R_L changes. The proposed method still works well when the motor load is included.

Similar to active power, the adaptive adjustment process of reactive power is outlined in Fig. 4. The difference is that Q_L could be negative due to the possible presence of capacitive loads, while the active power P_L is always non-negative.

It should be clarified that in the actual power adjustment process, the operating point of the load should be continuously changing in real time, which means that there should be no jumping from point A to point B and from point B to point C. The above operating point mutation-based analysis is used only for better illustration of the adjusting principle of the proposed reverse droop control strategy.

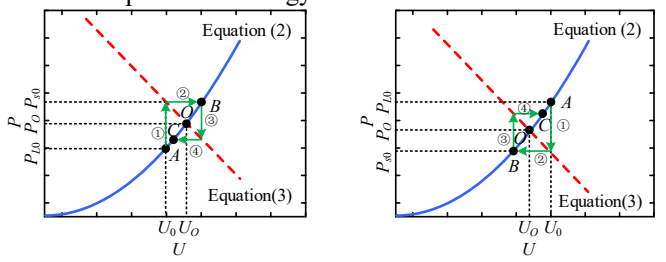

Fig. 3. Schematic diagram of the adaptive adjustment process of active power. (a) P_{s0}>P_{L0}. (b) P_{s0}<P_{L0}.

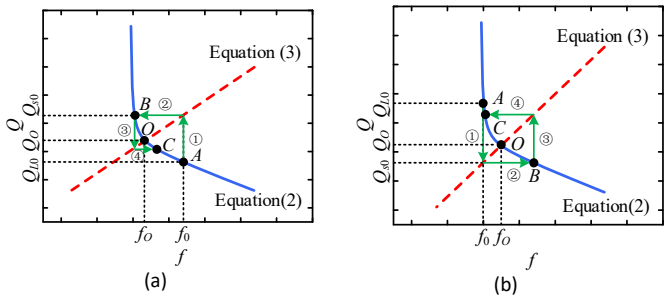

Fig. 4. Schematic diagram of the adaptive adjustment process of reactive power. (a) Q_{s0}>Q_{L0}. (b) Q_{s0}<Q_{L0}.

C. Integrated Control Strategy of the IFC

Based on the above analysis, the integrated control block diagram of the IFC is shown in Fig. 5. Where: U_d, U_q, I_{ld}, I_{lq}, I_d, I_q are the d-axis and q-axis components of the load voltage, the inductor current, and the inverter output current, respectively. The superscript * represents the corresponding reference value. $k_I(s) = k_{pI} + k_{iI}/s$ and $k_U(s) = k_{pU} + k_{iU}/s$ are the compensators of the current control loop and voltage control loop, respectively. The PLL in the proposed controller is based on the SRF-PLL [26], which is widely used to estimate the frequency and phase of the PCC voltage.

The control strategies of the IFC under various operating modes are revealed as follows.

(1) Under the grid-tied mode, the switches S_g and S_c in Fig. 1 are closed. Multiplexer#1 is thrown at "0" and multiplexer#2 switch is thrown at "2" in Fig. 5. Therefore, the IFC is controlled as a current source that outputs constant power.

(2) When islanding occurs, the switch S_g turns off, and S_c remains closed due to the islanding detection delay. In such a case, multiplexer#1 and multiplexer#2 are still at position "0" and "2" respectively, which means the reverse droop control is maintained. The voltage and frequency of critical loads will be kept by adaptively adjusting the IFC output power to the rated load power.

(3) After the completion of islanding detection, S_c also turns off. Multiplexer#1 is switched from "0" to "1" and multiplexer#2 is switched from "2" to "3," to realize the *V-f* control of the IFC. Thereby, the load voltage and frequency are controlled to the rated values. Correspondingly, the reverse droop control references P_s^* and Q_s^* are automatically restored to P_{s0} and Q_{s0}.

(4) When the main grid is recovered, i.e., S_g turns on. Multiplexer#2 is switched from "3" to "2." In this way, the pre-synchronization control [27] is put in to synchronize the voltage phase of the critical loads with the PCC voltage phase.

(5) After the pre-synchronization control is completed, S_c turns on. Multiplexer#1 is switched from "1" to "0" to achieve a constant power output of IFC under grid-tied mode.

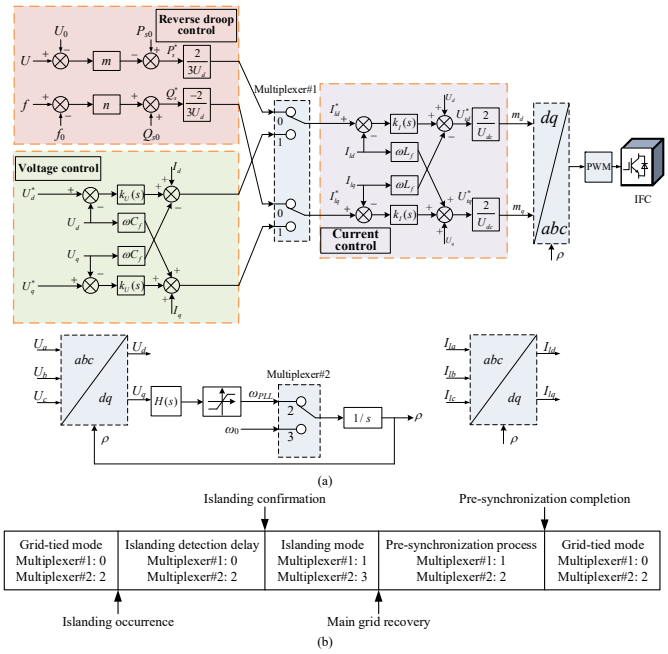

Fig. 5. The integrated control block diagram of the IFC and the block diagram of the transfer sequence. (a) The integrated control block. (b) The block diagram of the transfer sequence.

IV. Parameters Design and System Stability Analysis

A. Parameters of the Compensators

According to [28], the formulas to calculate the compensator parameters in the current loop are given as:

$$k_{pI} = L_f / \tau_i \,, \tag{4}$$

$$k_{iI} = R_f / \tau_i \,. \tag{5}$$

Where τ_i is the time constant of the current loop, which is generally selected as 0.5 ms~5 ms.

Also, the compensator parameters in the voltage loop can be obtained by the following formulas [29] as:

$$k_{pU} = \frac{C_f}{\tau_i}\left(\frac{1-\sin\gamma}{1+\sin\gamma}\right)^{\frac{1}{2}}, \tag{6}$$

$$k_{iU} = \frac{C_f}{\tau_i^2}\left(\frac{1-\sin\gamma}{1+\sin\gamma}\right)^{\frac{3}{2}}. \tag{7}$$

Where the phase margin γ is typically chosen as 40°~50°.

B. Droop Coefficients Design

The selection of the proper droop coefficients should ensure two basic requirements:

(1) The system should operate stably at point *O*.

(2) The voltage and frequency are within the allowable deviation range.

The selection methods of droop coefficients that satisfy the above conditions will be presented by the following derivations.

1) Stability Analysis

The equivalent circuit of the system during the islanding detection delay is shown in Fig. 6 with the current information added. Where i_l is the current of filter inductor, i_{LR}, i_{LC} and i_{LL} are the currents of resistive loads, capacitive loads and inductive loads respectively. It is noted that when IFC is

controlled as a current source, the filter capacitor can also be considered as part of the critical loads.

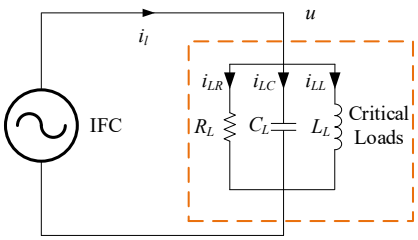

Fig. 6. The equivalent circuit of the system during the islanding detection delay.

With reference to Fig. 6, dynamics of the load voltage are described by the space-phasor equation:

$$\frac{\mathrm{d}}{\mathrm{d}t}\vec{i}_l=\frac{\mathrm{d}}{\mathrm{d}t}(\vec{i}_{LR}+\vec{i}_{LC}+\vec{i}_{LL})=\frac{1}{R_L}\frac{\mathrm{d}\vec{u}}{\mathrm{d}t}+C_L\frac{\mathrm{d}^2\vec{u}}{\mathrm{d}t^2}+\frac{\vec{u}}{L_L}. \quad (8)$$

Expressing each space phasor in (8) in terms of its *dq*-frame components, and applying Laplace transform to it, then the load voltage is obtained as:

$$\begin{cases} U_d=[sI_{ld}-\omega_{dq}I_{lq}+(2s\omega_{dq}C_L+\omega_{dq}/R_L)U_q] \\ \qquad R_LL_L/(s^2R_LL_LC_L+sL_L-\omega_{dq}^2R_LL_LC_L+R_L) \\ U_q=[sI_{lq}+\omega_{dq}I_{ld}-(2s\omega_{dq}C_L+\omega_{dq}/R_L)U_q] \\ \qquad R_LL_L/(s^2R_LL_LC_L+sL_L-\omega_{dq}^2R_LL_LC_L+R_L) \end{cases}. \quad (9)$$

Where ω_{dq} is the rotational angular frequency of *dq*-frame. If the PLL tracks the load voltage phase $\omega t+\theta$, then the term

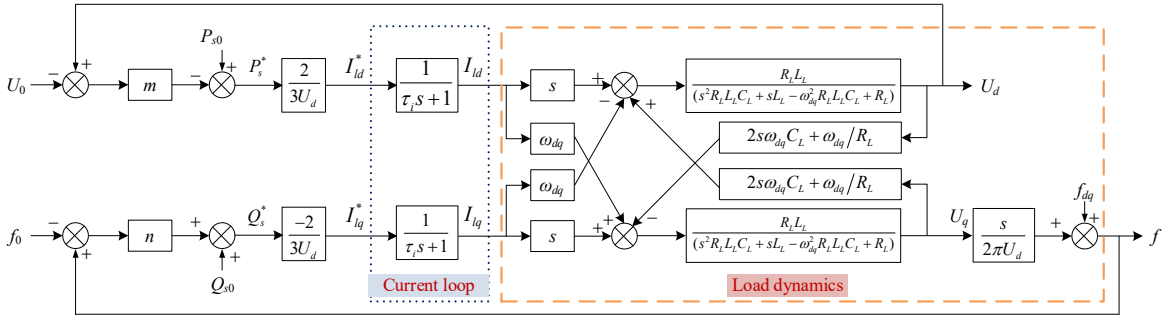

Fig. 7. The control block diagram of the proposal reverse power droop controller.

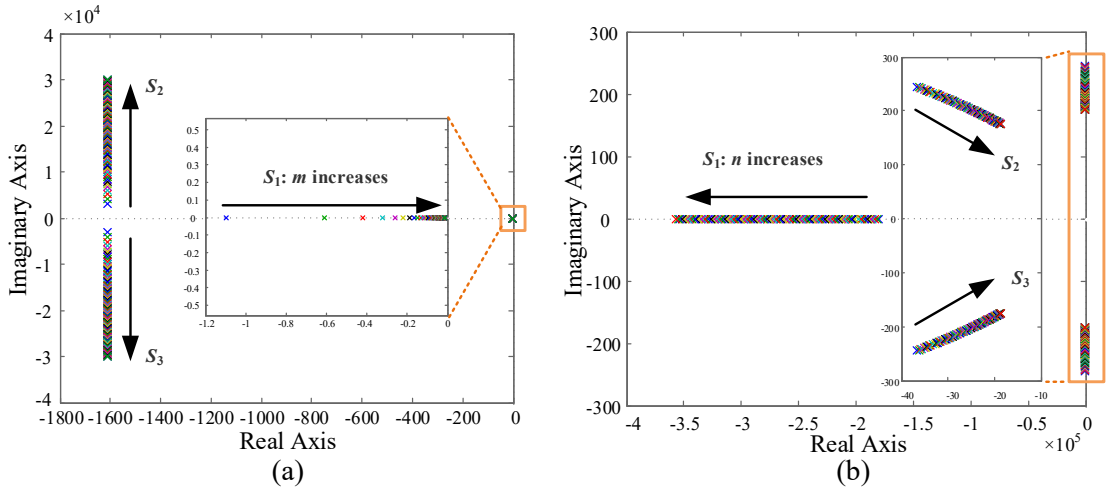

Fig. 8. The system root locus. (a) The root locus of the voltage loop at $m\in$[1 MW/kV, 100 MW/kV]. (b) The root locus of the frequency loop at $n\in$[1 MVar/Hz, 2 MVar/Hz].

$\omega t+\theta-\rho$ is close to zero, and we have [26]:

$$\begin{cases} u_d=U\cos(\omega t+\theta-\rho)\approx U \\ u_q=U\sin(\omega t+\theta-\rho)\approx U(\omega t+\theta-\rho) \end{cases}. \quad (10)$$

Where ρ is the rotation angle of *dq*-frame, and $\mathrm{d}\rho/\mathrm{d}t=\omega_{dq}$. Similarly, (10) can be expressed in the Laplace domain as:

$$\begin{cases} U=U_d \\ f=f_{dq}+U_q s/(2\pi U) \end{cases}. \quad (11)$$

In which $f=\omega/(2\pi)$ and $f_{dq}=\omega_{dq}/(2\pi)$. Based on (9), (11) and Fig. 5, the loop block diagram of the proposal reverse power droop controller is demonstrated in Fig. 7.

According to Fig. 7, the characteristic equations of the voltage loop and frequency loop are respectively presented as:

$$\begin{cases} 1+2mR_LL_Ls/[3U_d(\tau_i s+1)(s^2R_LL_LC_L+sL_L-\omega_{dq}^2R_LL_LC_L+R_L)]=0 \\ 1+2nR_LL_Ls^2/[6\pi U_d^2(\tau_i s+1)(s^2R_LL_LC_L+sL_L-\omega_{dq}^2R_LL_LC_L+R_L)]=0 \end{cases} \quad (12)$$

Assuming $U_d\approx U_0$ and $\omega_{dq}\approx\omega_0=2\pi f_0$ under a steady-state operating condition, then according to (12) and the parameters shown in Table I, the root locus of the system is depicted in Fig. 8 considering a variation of $m\in$[1 MW/kV, 100 MW/kV] and $n\in$[1 MVar/Hz, 2 MVar/Hz]. Fig. 8 shows that when the droop

coefficients m and n increase, the root locus remains in the left half s-plane, which indicates that the system endows superior stability in the range of concern. In particular, even when m is taken as 100 MW/kV and n is taken as 2 MVar/Hz, such large droop coefficients will not lead to system instability.

In addition, due to the inherent independence of the reverse droop control, the output power of the IFC is only dependent on load voltage and its own control parameters. This is to say, IFCs operate independently of each other. Therefore, as long as each IFC is stable, the system will be stable even with parallel-operated IFCs.

2) Voltage Quality Requirements

According to the IEEE std. 1547−2003 standard [30] related to the distributed generation's access to the power grid, the allowable deviation limits of the AC voltage and frequency are ± 7% U_0, and ± 0.2 Hz, respectively. Since the DC distribution network can be regarded as a distributed generation with a larger capacity, the aforementioned voltage quality requirements are also applicable to the interconnection of the AC and DC distribution networks.

According to (2) and (3), the active power balance equation when the load voltage converges at point O is (assume $P_s^*=P_s$):

$$P_{s0}-m(U_O-U_0)=\frac{U_O^2}{R_L}=\frac{U_O^2}{U_0^2}P_{L0}. \tag{13}$$

i.e.,

$$\begin{aligned} m&=(P_{s0}-\frac{U_O^2}{U_0^2}P_{L0})\Big/(U_O-U_0)\\ &=\begin{cases}[P_{s0}-(1+\Delta U\%)^2P_{L0}]/(\Delta U\%U_0), & P_{s0}>P_{L0}\\ [(1-\Delta U\%)^2P_{L0}-P_{s0}]/(\Delta U\%U_0), & P_{s0}<P_{L0}\end{cases}\end{aligned}. \tag{14}$$

Where $0\le\Delta U\%\le 0.07$ signifies the offset of the voltage. Equation (14) manifests that when $\Delta U\%$ reaches the maximum value of 0.07, the corresponding m has a minimum value, i.e., the constraint formula of m is:

$$m\ge\begin{cases}(P_{s0}-1.07^2P_{L0})/(0.07U_0), & P_{s0}>P_{L0}\\ (0.93^2P_{L0}-P_{s0})/(0.07U_0), & P_{s0}<P_{L0}\end{cases}. \tag{15}$$

It should be noted that if $(P_{s0}-1.07^2P_{L0})$ or $(0.93^2P_{L0}-P_{s0})$ is less than 0, which indicates that P_{s0} and P_{L0} are very close, thus m can be taken as an arbitrary non- negative value to meet the requirement of the voltage magnitude.

Similarly, the reactive power balance equation when the frequency converges at point O is (assume $Q_s^*=Q_s$):

$$Q_{s0}+n(f_O-f_0)=U^2(\frac{1}{2\pi f_OL_L}-2\pi f_OC_L). \tag{16}$$

Assuming that the load voltage U is stabilized at U_O by the regulation of active power, then it yields to:

$$\begin{aligned} n&=[U_O^2(\frac{1}{2\pi f_OL_L}-2\pi f_OC_L)-Q_{s0}]\Big/(f_O-f_0)\\ &=\begin{cases}\left\{Q_{s0}-U_O^2[\frac{1}{2\pi(1-\Delta f\%)f_0L_L}-2\pi(1-\Delta f\%)f_0C_L]\right\}\Big/(\Delta f\%f_0), & Q_{s0}>Q_{L0}\\ \left\{U_O^2[\frac{1}{2\pi(1+\Delta f\%)f_0L_L}-2\pi(1+\Delta f\%)f_0C_L]-Q_{s0}\right\}\Big/(\Delta f\%f_0), & Q_{s0}<Q_{L0}\end{cases}\end{aligned}. \tag{17}$$

Where $0\le\Delta f\%\le 0.004$ denotes the offset of the frequency. Equation (17) declares that when $\Delta f\%$ reaches the maximum value of 0.004, the corresponding n has a minimum value, i.e., the constraint formula of n can be determined as:

$$n\ge\begin{cases}[Q_{s0}-U_O^2(\frac{1}{1.992\pi f_0L_L}-1.992\pi f_0C_L)]\Big/(0.004f_0), & Q_{s0}>Q_{L0}\\ [U_O^2(\frac{1}{2.008\pi f_0L_L}-2.008\pi f_0C_L)-Q_{s0}]\Big/(0.004f_0), & Q_{s0}<Q_{L0}\end{cases}. \tag{18}$$

The rated reactive power delivered by the IFC is typically set as 0, i.e., Q_{s0}=0. Thus, when the critical loads are capacitive or inductive, (30) can be further simplified as:

$$n\ge\begin{cases}U_O^21.992\pi f_0C_L/(0.004f_0)\approx -0.996Q_{L0}/(0.004f_0), & Q_{L0}<0\\ U_O^2\dfrac{1}{2.008\pi f_0L_L}\Big/(0.004f_0)\approx\dfrac{1}{1.004}Q_{L0}\Big/(0.004f_0), & Q_{L0}>0\end{cases}. \tag{19}$$

From (15) and (19), it can be seen that a larger m and a larger n guarantee better voltage quality. However, according to (3), they also render the output power of the IFC to be sensitive to voltage and frequency fluctuations under the grid-tied mode. Thus, the values of m and n are recommended to be in a moderate range.

V. Simulation and Experimental Verifications

A. Simulation Results

To verify the effectiveness of the proposed control strategy, the Suzhou hybrid distribution network of the National Key R&D Program of China is shown in Fig. 9, the detailed model is developed in the professional software PSCAD/EMTDC. Three sub-systems, including two AC distribution networks and one DC distribution network are depicted in Fig. 9. The AC distribution networks are connected to the DC distribution network through two IFCs. Since the DC voltage U_{dc} is 20 kV, modular-multilevel converters are adopted. Herein, the IFC-2 is employed to support the voltage of the DC distribution network, whereas IFC-1 controls the power flow between sub-systems. The switch S_{dc} offers diversity in the operation of the DC distribution network. The main objective of this research study is to achieve an uninterrupted and qualified power supply to the critical AC loads, which is performed by switching the control strategy of IFC-1 when the main grid-1 exits due to maintenances or failures. The related circuit parameters and control parameters are shown in Table I.

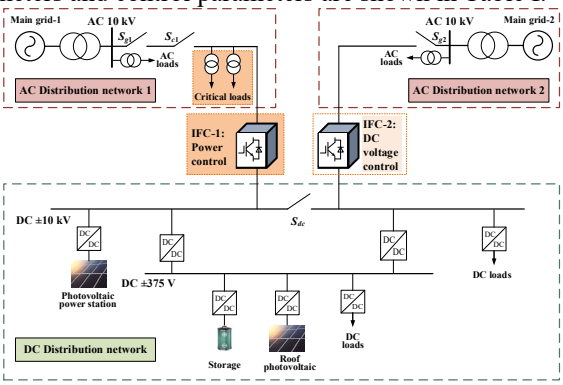

Fig. 9 Topology of Suzhou hybrid distribution network pilot project.

TABLE I
Simulation Parameters

Circuit parameters	Value	Control parameters	Value
DC voltage U_{dc}	20 kV	Reference active	3 MW

AC rated voltage U_N	10 kV	power P_{s0} Reference reactive power Q_{s0}	0 MVar
AC phase voltage amplitude U_0	8.165 kV	Reference voltage U_d^*	8.165 kV
AC rated frequency f_0	50 Hz	Reference frequency f^*	50 Hz
Filter resistor R_f	120 mΩ	Time constant τ_i	1 ms
Filter inductor L_f	0.935 mH	Current loop P coefficient k_{pI}	0.935
Filter capacitor C_f	9 uF	Current loop I coefficient k_{iI}	120
Load resistance R_L	50 Ω	Voltage loop phase margin γ	45°
Load inductance L_L	1000 mH	Voltage loop P coefficient k_{pU}	0.00373
Load capacitance C_L	9 uF	Voltage loop I coefficient k_{iU}	0.640
Load rated active power P_{L0}	2.00 MW	Voltage droop coefficient m	10 MW/kV
Load rated active power Q_{L0}	0.036 MVar	Frequency droop coefficient n	1.5 MVar/Hz

1) The Transition from the Grid-tied Mode to the Islanding Mode

Active islanding detection methods can be applied to detect islanding [17]. Assuming the islanding detection delay is 0.2 s, then the simulation process can be separated into the following two stages:

(1) The IFC is initially connected to the grid and is controlled as a current source, however, at t =1.5 s, the islanding occurs and S_g turns off.

(2) The detection time of islanding is from t =1.5 s to t =1.7 s. At t =1.7 s the islanding detection is completed, S_c turns off and the IFC switches to be a controlled voltage source.

The simulation results with the conventional constant power control are shown in Fig. 10. In a conventional constant power control, the IFC is controlled to output constant power P_{s0}+jQ_{s0} to the critical loads, even when islanding occurs. In this case, when the islanding occurs at t =1.5 s, P_{s0} is greater than P_{L0}, which causes the load voltage magnitude to rise to 10 kV. Similarly, the frequency also increases and exceeds the maximum limit of 50.2 Hz since Q_{s0} is less than Q_{L0}. Hence, the load voltage and frequency during the islanding detection delay are unacceptable.

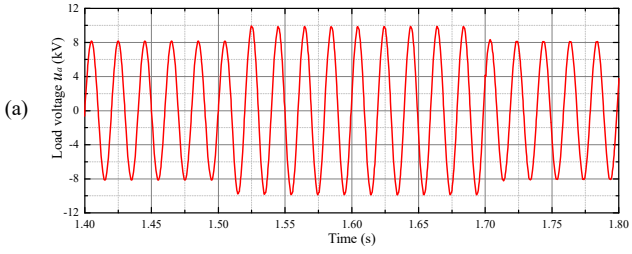

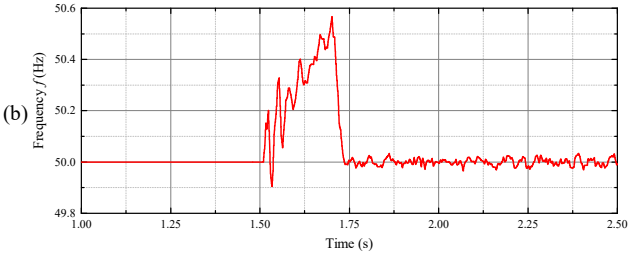

Fig. 10 Simulation waveforms with conventional control. (a) Load voltage. (b) Frequency waveform.

The simulation waveforms using the proposed reverse droop control are shown in Fig. 11. It can be observed from Fig. 11(a) and Fig. 11(b) that the IFC initially injects a constant power P_{s0}+jQ_{s0}. When islanding is triggered at t =1.5 s, P_s+jQ_s is adaptively adjusting to the rated load power P_{L0}+jQ_{L0}. Thus, the magnitude and frequency of the load voltage are maintained within the allowable deviation range, as shown in Fig. 11(c) and Fig. 11(d). At t =1.7 s, when the islanding is confirmed, the IFC is switched from reverse droop control to *V-f* control. In this case, the load voltage and frequency are re-controlled to the rated values, and the reference power value of the droop control is automatically restored to P_{s0}+jQ_{s0}. It can be concluded that the IFC output power decreases according to the surplus of power with the proposed reverse droop control. The proposed method is effective to improve the voltage quality without harmful transients.

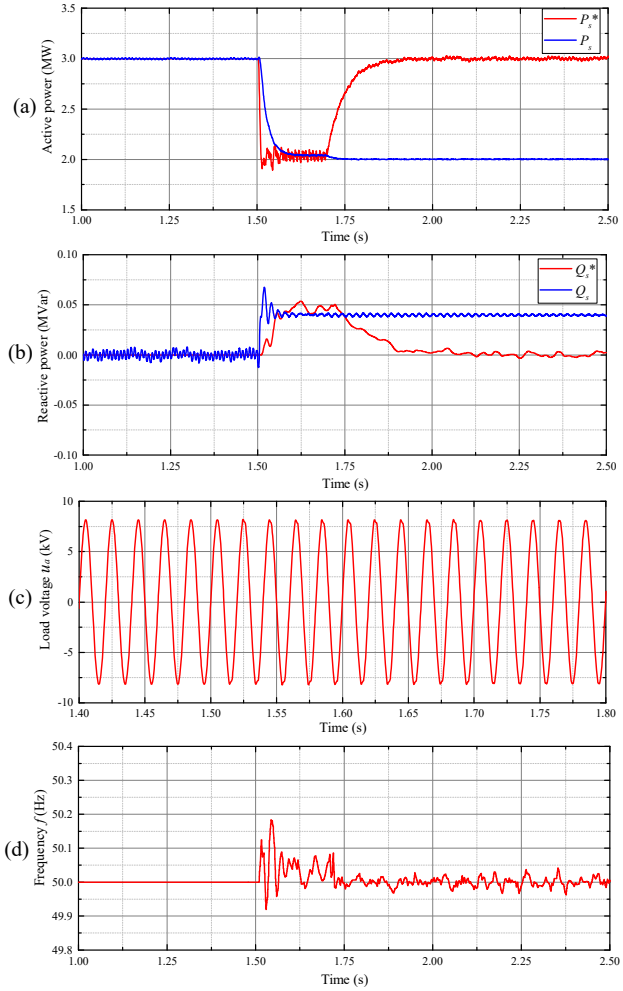

Fig. 11 Simulation waveforms with the proposed reverse droop control. (a) Active power. (b) Reactive power. (c) Load voltage. (d) Frequency waveform.

2) The Transition from the Islanding Mode to the Grid-tied Mode

The simulation process from the islanding mode to the grid-tied mode can also be divided into two stages.

(1) The IFC is initially controlled as a voltage source, however, at t =2.5 s, the main grid is recovered, S_g turns on and the pre-synchronization control activates.

(2) At t =2.7 s, the pre-synchronization is completed, S_c turns on and the IFC switches back to be a controlled current source.

The simulation waveforms are presented in Fig. 12. The load voltage u_a and grid voltage u_{ga} during the pre-synchronization process are shown in Fig. 12(a). Before t =2.5 s, the pre-synchronization control has not been adopted, the phase of the IFC output voltage deviates from the phase of grid voltage. However, when the pre-synchronization control is applied at t =2.5 s, the synchronization is realized within 0.1 s. Fig. 12(b) and (c) indicate that the IFC output power is automatically back to P_{s0}+jQ_{s0} under the grid-tied mode after t = 2.7 s.

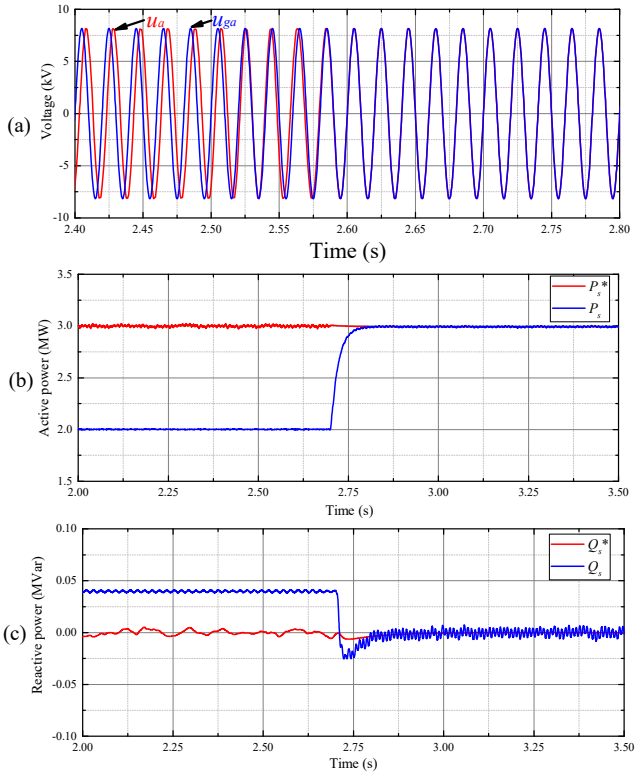

Fig. 12 Transients from the islanding mode to the grid-tied mode. (a) Voltages of pre-synchronization control. (b) Active power. (c) Reactive power.

B. Experimental Results

To verify the proposed control strategy, a scaled-down experimental platform is built based on TI's TMS320F28335, which is illustrated in Fig. 13. The parameters are shown in Table II. Since the conditions that P_{s0}> P_{L0} and Q_{s0}<Q_{L0} are certified by simulations, hereby, P_{s0}< P_{L0} and Q_{s0}>Q_{L0} conditions are investigated in detail through experiments.

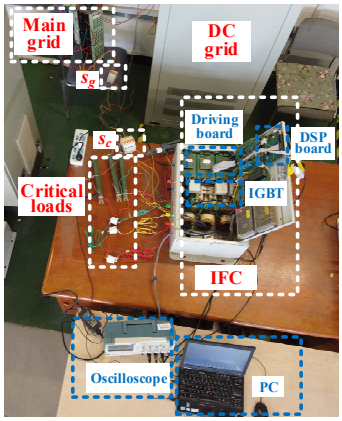

Fig. 13 A scaled-down experimental platform.

TABLE II
EXPERIMENTAL PARAMETERS

Circuit parameters	Value	Control parameters	Value
DC voltage U_{dc}	200 V	Reference active power P_{s0}	168.75 W
AC rated voltage U_N	53 V	Reference reactive power Q_{s0}	0 Var
AC phase voltage amplitude U_0	75 V	Reference voltage U_d^*	75 V
AC rated frequency f_0	50 Hz	Reference frequency f^*	50 Hz
Filter resistor R_f	78.25 mΩ	Time constant τ_i	1 ms
Filter inductor L_f	0.54 mH	Current loop P coefficient k_{pI}	0.54
Filter capacitor C_f	9 uF	Current loop I coefficient k_{iI}	78.25
Load resistance R_L	25 Ω	Voltage loop phase margin γ	45°
Load inductance L_L	0 mH	Voltage loop P coefficient k_{pU}	0.00373
Load capacitance C_L	39 uF	Voltage loop I coefficient k_{iU}	0.640
Load rated active power P_{L0}	337.5 W	Voltage droop coefficient m	50 W/V
Load rated active power Q_{L0}	-79.6 MVar	Frequency droop coefficient n	300 Var/Hz

1) The Transition from the Islanding Mode to the Grid-tied Mode

As in the simulations, the experiments are performed in two stages:

(1) First, the IFC is connected to the main grid and is controlled as a current source, then the islanding occurs and the switch S_g turns off.

(2) Secondly, the islanding gets confirmed, the switch S_c turns off and the IFC switches to V-f control.

In the first stage, Fig. 14 shows the experimental results when the IFC is controlled by the conventional constant power control. Fig. 15 exhibits the experimental results when the proposed reverse droop control is applied. For both Fig. 14 and Fig. 15, the grid-tied current i_{ga} drops to 0 denotes the triggering of islanding. In Fig. 14, the magnitude and frequency of the load voltage decrease to 53 V and 40 Hz respectively due to

$P_{s0}< P_{L0}$ and $Q_{s0}>Q_{L0}$. These deteriorations are caused by the mismatch between P_{s0}+jQ_{s0} and P_{L0}+jQ_{L0}. Furthermore, in Fig. 15, the output power of the IFC is adaptively adjusted to the rated load power P_{L0}+jQ_{L0} with the proposed reverse droop control. Thus, the load voltage magnitude and frequency are maintained within the allowable deviation range. The proposed reverse droop control significantly improves the quality of voltage and frequency as compared to the traditional constant power control.

It should be noted that the poor quality of the grid-tied current waveform is caused by the weak AC grid with a large number of nonlinear devices. The current harmonics generated by these nonlinear devices introduces a large number of harmonics into the PCC voltage through the line impedance [30]-[33]. Thus, the grid-tied current is distorted. In addition, the experimental platform we built is a scaled-down version, whose grid-tied current magnitude is only about 2A. This makes the distortion effect of harmonics on the grid-tied current more obvious. Various literature have analyzed this phenomenon and proposed several methods to suppress the harmonic distortion of the grid-tied current [31]-[33].

Another phenomenon that needs to be explained is the reactive power oscillation under the grid-tied mode, as shown in Fig. 15 (a). The reason is that there is an error between the PLL output phase and the PCC voltage phase during the IFC start-up transient. Due to the resistive line in the low voltage grid, this phase error causes reactive power to oscillate under the grid-tied mode. However, the reactive power oscillation disappears in the steady state. As can be seen from Fig. 17, the reactive power does not oscillate after the pre-synchronous is completed.

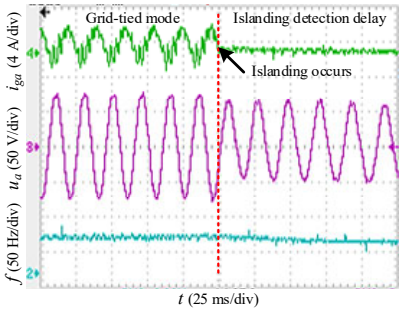

Fig. 14 Experimental waveforms with conventional control.

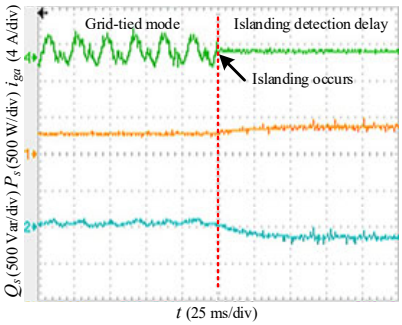

(a)

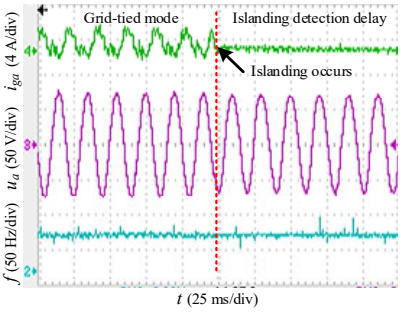

(b)

Fig. 15 Experimental waveforms with the proposed reverse droop control. (a) Power waveforms. (b) Voltage and frequency waveforms.

In the second stage, the islanding detection is completed and the mode switching signal, i.e., *Flag-mode*, which steps from 0 to 1, is shown in Fig. 16. This leads to the turning off of switch S_c and the changing of the IFC to the *V-f* control. As observed in Fig. 16, the load voltage waveform changes smoothly.

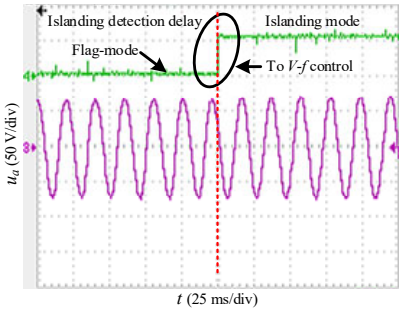

Fig. 16 Experimental waveforms when the IFC is switched from reverse droop control to *V-f* control.

2) The Transition from the Islanding Mode to the Grid-tied Mode

There are two main stages to achieve the transition from the islanding mode to the grid-tied mode.

(1) First, the IFC is with *V-f* control during islanding mode. However, when the main grid is recovered, the switch S_g turns on and pre-synchronization control is applied.

(2) Secondly, after the completion of synchronization, the switch S_c turns on while the IFC switches to reverse droop control.

The experimental results are shown in Fig. 17. The synchronization signal is denoted as *Flag-syn* in Fig. 17(a), when it steps from 0 to 1, the pre-synchronization control activates and the load voltage synchronizes with the grid voltage. Fig. 17(b) presents the waveforms of the grid-tied current, load voltage, IFC output active and reactive power when the IFC is switching from the *V-f* control to the reverse droop control. It is noted that there is no voltage distortion during the transition process. Under the grid-tied mode, the output power of the IFC is smoothly tracked back to the reference power P_{s0}+jQ_{s0}. Since the power flows from the main grid to the critical loads, the phase angle of the grid-tied current i_{ga} remains opposite to the phase angle of the load voltage.

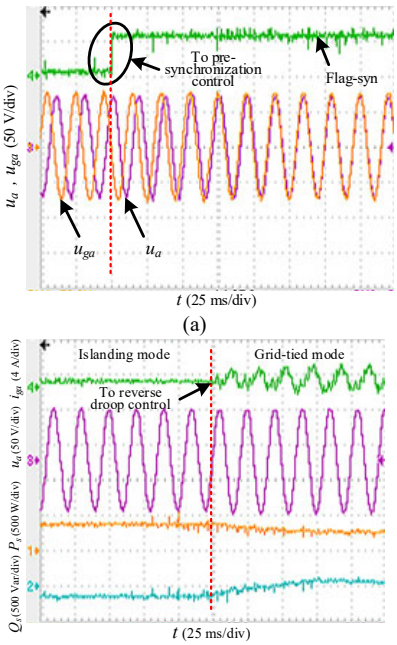

Fig.17 Experimental waveforms from the islanding mode to the grid-tied mode. (a) Waveforms when pre-synchronization control is applied. (b) Waveforms when the IFC is switched from *V-f* control to reverse droop control.

VI. CONCLUSION

In this paper, a reverse droop control-based strategy is proposed to realize smooth transfers between the grid-tied mode and islanding mode for IFCs in AC/DC hybrid distribution networks. By adaptively tracking the IFC output power to the rated load power, the proposed control strategy enables an uninterrupted and qualified power supply to AC critical loads during islanding detection delays. In addition, a universal parameter design method is presented based on the stability analysis and the voltage quality requirements. Compared with the existing methods either suffering from poor voltage quality or complex structures, the proposed method facilitates smooth transitions in a simple but effective approach. Also, it is convenient for engineering implementation. Simulation and experimental results clearly validate the excellent behavior of the proposed control strategy.

REFERENCES

[1] G. Bathurst, G. Hwang, and L. Tejwani, "MVDC-the new technology for distribution networks," in *Proceedings of the 11th IET International Conference on AC and DC Power Transmission*, Birmingham, 2015, pp. 1–5.

[2] S. Tang, M. Chen, G. Jia and C. Zhang, "Topology of current-limiting and energy-transferring DC circuit breaker for DC distribution networks," *CSEE Journal of Power and Energy Systems*, vol. 6, no. 2, pp. 298-306, June 2020.

[3] M. X. Han, D. Xu, and L. Wan, "Hierarchical optimal power flow control for loss minimization in hybrid multi-terminal HVDC transmission system," *CSEE Journal of Power and Energy Systems*, vol. 2, no. 1, pp. 40–46, Mar. 2016.

[4] L. Jia, Y. Zhu, S. Du and Y. Wang, "Analysis of the transition between multiple operational modes for hybrid AC/DC microgrids," *CSEE Journal of Power and Energy Systems*, vol. 4, no. 1, pp. 49-57, March 2018.

[5] C. Kumar and M. Liserre, "A new prospective of smart transformer application: dual microgrid (DMG) operation," in *Proceedings of the IECON 2015-41st Annual Conference of the IEEE Industrial Electronics Society*, Yokohama, 2015, pp. 004482–004487.

[6] X. Li, H. Y. Zhang, M. B. Shadmand, and R. S. Balog, "Model predictive control of a voltage-source inverter with seamless transition between islanded and grid-connected operations," *IEEE Transactions on Industrial Electronics*, vol. 64, no. 10, pp. 7906–7918, Oct. 2017.

[7] X. Li, H. Y. Zhang, and R. Balog, "Control strategy for seamless transfer between island and grid-connected operation for a dual-mode photovoltaic inverter," in *Proceedings of the 2015 IEEE Energy Conversion Congress and Exposition (ECCE)*, Montreal, QC, 2015, pp. 5983–5990.

[8] S. S. Huang, Y. Konishi, Z. Z. Yang, and M. J. Hsieh, "Observer-based capacitor current sensorless control applied to a single-phase inverter system with seamless transfer," *IEEE Transactions on Power Electronics*, vol. 34, no. 3, pp. 2819–2828, Mar. 2019.

[9] S. Yoon, J. Kwon, J. Park, and S. Choi, "Indirect current control for seamless transfer of three-phase utility interactive inverters," in *Proceedings of the 2011 Twenty-Sixth Annual IEEE Applied Power Electronics Conference and Exposition (APEC)*, Fort Worth, TX, 2011, pp. 625–632.

[10] S. Yoon, H. Oh, and S. Choi, "Controller design and implementation of indirect current control based utility-interactive inverter system," *IEEE Transactions on Power Electronics*, vol. 28, no. 1, pp. 26–30, Jan. 2013.

[11] Z. Liu and J. J. Liu, "Indirect current control based seamless transfer of three-phase inverter in distributed generation," *IEEE Transactions on Power Electronics*, vol. 29, no. 7, pp. 3368–3383, Jul. 2014.

[12] F. Gao and M. R. Iravani, "A control strategy for a distributed generation unit in grid-connected and autonomous modes of operation," *IEEE Transactions on Power Delivery*, vol. 23, no. 2, pp. 850–859, Apr. 2008.

[13] Z. Q. Guo, D. S. Sha, and X. Z. Liao, "Voltage magnitude and frequency control of three-phase voltage source inverter for seamless transfer," *IET Power Electronics*, vol. 7, no. 1, pp. 200–208, Jan. 2014.

[14] J. Wang, N. C. P. Chang, X. W. Feng, and A. Monti, "Design of a generalized control algorithm for parallel inverters for smooth microgrid transition operation," *IEEE Transactions on Industrial Electronics*, vol. 62, no. 8, pp. 4900–4914, Aug. 2015.

[15] *IEEE Recommended Practice for Utility Interface of Photovoltaic（PV）Systems*, IEEE Std 929-2000, 2000.

[16] *IEEE Guide for Monitoring, Information Exchange, and Control of Distributed Resources Interconnected With Electric Power Systems*, IEEE 1547.3-2007, 2007.

[17] P. Deshbhratar, R. Somalwar, and S. G. Kadwane, "Comparative analysis of islanding detection methods for multiple DG based system," in *Proceedings of 2016 International Conference on Electrical, Electronics, and Optimization Techniques (ICEEOT)*, Chennai, 2016, pp. 1525–1530.

[18] J. R. Chen, F. Milano, and T. O'Donnell, "Assessment of grid-feeding converter voltage stability," *IEEE Transactions on Power Systems*, vol. 34, no. 5, pp. 3980–3982, Sep. 2019.

[19] D. Wu, F. Tang, J. C. Vasquez, and J. M. Guerrero, "Control and analysis of droop and reverse droop controllers for distributed generations," in *Proceedings of 2014 IEEE 11th International Multi-Conference on Systems, Signals & Devices (SSD14)*, Barcelona, 2014, pp. 1–5.

[20] S. Y. Mousazadeh Mousavi, A. Jalilian, M. Savaghebi, and J. M. Guerrero, "Autonomous control of current- and voltage-controlled DG interface inverters for reactive power sharing and harmonics compensation in islanded microgrids," *IEEE Transactions on Power Electronics*, vol. 33, no. 11, pp. 9375–9386, Nov. 2018.

[21] J. M. Guerrero, J. Matas, L. G. de Vicuna, M. Castilla, and J. Miret, "Decentralized control for parallel operation of distributed generation inverters using resistive output impedance," *IEEE Transactions on Industrial Electronics*, vol. 54, no. 2, pp. 994–1004, Apr. 2007.

[22] J. C. Vasquez, R. A. Mastromauro, J. M. Guerrero, and M. Liserre, "Voltage support provided by a droop-controlled multifunctional inverter," *IEEE Transactions on Industrial Electronics*, vol. 56, no. 11, pp. 4510–4519, Nov. 2009.

[23] H. U. May Marma and X. D. Liang, "Composite load model and transfer function based load model for high motor composition load," in *Proceedings of 2019 IEEE Electrical Power and Energy Conference (EPEC)*, Montreal, QC, Canada, 2019, pp. 1–5.

[24] L. Amber, T. H. Ortmeyer, and P. McGrath, "Modeling induction machines and core-form transformers in unbalanced distribution circuits," in *Proceedings of 2014 IEEE PES General Meeting | Conference & Exposition*, National Harbor, MD, 2014, pp. 1–5.

[25] Y. J. Lin, Z. W. Xu, and W. C. Xie, "Asynchronous motor's more-accurate equivalent circuit parameter determining by auto 2fit," in *Proceedings of 2010 International Conference on Electrical Machines and Systems*, Incheon, 2010, pp. 1417–1420.

[26] A. Yazdani and R Iravani, "Grid-imposed frequency VSC system: control in *dq*-frame," in *Voltage-Sourced Converters in Power Systems: Modeling, Control, and Applications*, Hoboken: Wiley-IEEE Press, 2010, pp. 211–217.
[27] T. L. Vandoorn, B. Meersman, J. D. M. De Kooning, and L. Vandevelde, "Transition from islanded to grid-connected mode of microgrids with voltage-based droop control," *IEEE Transactions on Power Systems*, vol. 28, no. 3, pp. 2545–2553, Aug. 2013.
[28] A. Yazdani and R Iravani, "Grid-imposed frequency VSC system: control in *dq*-frame," in *Voltage-Sourced Converters in Power Systems: Modeling, Control, and Applications*, Hoboken: Wiley-IEEE Press, 2010, pp. 219–223.
[29] A. Yazdani and R. Iravani, "Controlled-frequency VSC system," in *Voltage-Sourced Converters in Power Systems: Modeling, Control, and Applications*, Hoboken: Wiley-IEEE Press, 2010, pp. 245–269.
[30] *IEEE Standard for Interconnecting Distributed Resources with Electric Power Systems*, IEEE Std 1547-2003, 2003.
[31] M. Liserre, R. Teodorescu, and F. Blaabjerg, "Stability of photovoltaic and wind turbine grid-connected inverters for a large set of grid impedance values," *IEEE Transactions on Power Electronics*, vol. 21, no. 1, pp. 263–271, Jan. 2006.
[32] J. M. Xu, S. J. Xie, Q. Qian, and B. F. Zhang, "Adaptive feedforward algorithm without grid impedance estimation for inverters to suppress grid current instabilities and harmonics due to grid impedance and grid voltage distortion," *IEEE Transactions on Industrial Electronics*, vol. 64, no. 9, pp. 7574–7586, Sep. 2017.
[33] W. Zhang, H. P. Liu, and W. Wang, "Harmonic suppression strategy for voltage-controlled grid-connected inverter based on parameter optimization," in *Proceedings of 2017 IEEE Transportation Electrification Conference and Expo, Asia-Pacific (ITEC Asia-Pacific)*, 2017.

Wenyuan Cao (S'19) was born in Hunan, China, in 1994. He received the B. S. degree in North China Electric Power University, Beijing, China, in 2017, where he is pursuing the Ph.D. degree, majoring in electrical engineering.
He is currently a guest Ph.D. student in the Department of Energy Technology, Aalborg University, Aalborg, Denmark. His research interests include hybrid AC/DC distribution network and its control.

Minxiao Han (M'05–SM'18) was born in Shannxi, China, in 1963. He received his Ph.D. from North China Electric Power University (NCEPU). He was a visiting Ph.D. student with Queen's University of Belfast, U.K. and a post-doctoral fellow with Kobe University, Japan. He is presently the Director of Institute of Flexible Electric Power Technology of NCEPU. He has been the leader in projects consigned by National Nature Science Foundation of China, National Educational Ministry, and enterprises. He has four published books and more than 100 refereed publications in journals and conferences. His research interests are the applications of power electronics in power system including HVDC, FACTS, power conversion and control.

Xiangkun Meng was born in Henan, China, in 1997. He received the B. S. degree in North China Electric Power University, Beijing, China, in 2019, where he is pursuing the master degree.
His research interests include the control of DC/AC converter and DC/DC converter.

Wenqiang Xie was born in Jiangsu, China, in 1993. He received the B.S. degree in North China Electric Power University, Beijing, China, in 2016, where he is pursuing the Ph.D. degree, majoring in electrical engineering.
His research interests include power electronics, control, and their applications in dc microgrids.

ZMARRAK WALI KHAN received his B.Sc. degree in Electrical Engineering from COMSATS University, Abbottabad, Pakistan in 2013, and M.Sc. degree in Electrical Engineering from CECOS University, Peshawar, Pakistan in 2016. He is currently pursuing PHD degree in the field of Electrical Engineering from the School of Electrical and Electronics Engineering, North China Electric Power University, China. His current interest lies in the field of VSC-HVDC, MMC-HVDC and high power dc-dc converters

Josep M. Guerrero (S'01–M'04–SM'08–F'15) received the B.S. degree in telecommunications engineering, the M.S. degree in electronics engineering, and the Ph.D. degree in power electronics from the Technical University of Catalonia, Barcelona, in 1997, 2000 and 2003, respectively. Since 2011, he has been a Full Professor with the Department of Energy Technology, Aalborg University, Denmark, where he is responsible for the Microgrid Research Program. From 2014, he is Chair Professor in Shandong University. Since 2015, he has been a Distinguished Guest Professor at Hunan University. Since 2016, he has been a visiting professor fellow at Aston University, UK, and a guest Professor at the Nanjing University of Posts and Telecommunications. From 2019, he became a Villum Investigator by The Villum Fonden, which supports the Center for Research on Microgrids (CROM) at Aalborg University, where he is the Founder and Director. He has published more than 500 journal papers in the fields of microgrids and renewable energy systems, which are cited more than 50,000 times. His research interests include

different microgrid aspects, including power electronics, distributed energy-storage systems, hierarchical and cooperative control, energy management systems, smart metering and the internet of things for ac/dc microgrid clusters and islanded minigrids, with a special focus on microgrid technologies applied to offshore wind and maritime microgrids for electrical ships, vessels, ferries, and seaports. Prof. Guerrero is an Associate Editor for a number of IEEE Transactions. He received the Best Paper Award of the IEEE TRANSACTIONS ON ENERGY CONVERSION for the period 2014–2015, the Best Paper Prize of IEEE-PES in 2015, the Best Paper Award of the IEEE JOURNAL OF POWER ELECTRONICS in 2016. From 2014 to 2019, he was awarded by Clarivate Analytics (former Thomson Reuters) as Highly Cited Researcher. In 2015, he was promoted as a Fellow at the IEEE for his contributions on distributed power systems and microgrids.

Gibran David Agundis Tinajero received the B.S. degree in mechanical and electrical engineering from the Universidad Autónoma de San Luis Potosí, San Luis Potosí, México, in 2012, and the M.Sc. and Ph.D. degrees in electrical engineering from the Universidad Autónoma de San Luis Potosí, San Luis Potosí, México, in 2014 and 2018, respectively. He is currently working as a Postdoctoral Fellow at the Energy Technology Department, Aalborg University, Denmark, where he contributes in different renewable-energy related projects. His research interests include modelling, analysis, and control of microgrid clusters including LV and MV distribution grids.